Ar and CH4 van der Waals complexes of 1 and 2fluoronaphthalene: A perturbed spherical top attached to a surface

B. B. Champagne, J. F. Pfanstiel, D. W. Pratt, and R. C. Ulsh

Citation: The Journal of Chemical Physics **102**, 6432 (1995); doi: 10.1063/1.469358
View online: http://dx.doi.org/10.1063/1.469358
View Table of Contents: http://scitation.aip.org/content/aip/journal/jcp/102/16?ver=pdfcov
Published by the AIP Publishing

Ar and CH_4 van der Waals complexes of 1- and 2-fluoronaphthalene: A perturbed spherical top attached to a surface

B. B. Champagne, J. F. Pfanstiel, and D. W. Pratt
Department of Chemistry, University of Pittsburgh, Pittsburgh, Pennsylvania 15260

R. C. Ulsh
Department of Chemistry, University of Pittsburgh, Johnstown, Pennsylvania 15904

(Received 1 July 1994; accepted 17 January 1995)

We compare and contrast the low and high resolution $S_1 \leftarrow S_0$ fluorescence excitation spectra of four van der Waals complexes, Ar–1FN, CH_4–1FN, Ar–2FN, and CH_4–2FN (where 1FN and 2FN are 1- and 2-fluoronaphthalene, respectively) in the gas phase. Whereas the Ar and CH_4 complexes exhibit comparable low resolution spectra, their high resolution spectra are significantly different. The CH_4–1/2FN complexes exhibit origin bands that are each split into three distinct subbands with different intensities and separations of less than 1 cm^{-1}. No such splittings are observed in Ar–1/2FN. The relative intensities of the three subbands in both CH_4 complexes are 1:2:2. These are identical, within experimental error, to the total statistical weights of the $J=0$, 1, and 2 rotational levels of CH_4. Both Ar and CH_4 are weakly attached to 1/2FN at a distance of ~3.5 Å above the aromatic plane. This distance decreases slightly (~0.1 Å) on $S_1 \leftarrow S_0$ excitation. Thus, the splittings observed in CH_4–1/2FN are attributed to ''surface-induced'' perturbations of the normally isotropic rotational motion of methane whose magnitudes depend on the electronic structure of the surface to which it is attached. A model is proposed that accounts for these observations. Comparison of the numerical predictions of this model with the experimental results shows that the rotational motion of the attached CH_4 is nearly the same as that of the free molecule. © *1995 American Institute of Physics.*

I. INTRODUCTION

Interest in the structural and dynamical properties of van der Waals complexes continues to motivate a large number of experimental and theoretical investigations. To a significant degree, these have focused on rare gas complexes of aromatic molecules, studies pioneered by Levy and co-workers.[1] But subsequent work has shown that van der Waals complexes can be formed between almost any pair of nonreacting species in a molecular beam, and can be characterized using a variety of spectroscopic techniques. Analyses of these spectra provide unique information about intermolecular forces.[2]

In this report, we apply the technique of $S_1 \leftarrow S_0$ fluorescence excitation spectroscopy to four van der Waals complexes, Ar–1-fluoronaphthalene (Ar–1FN), Ar–2-fluoronaphthalene (Ar–2FN), CH_4–1-fluoronaphthalene (CH_4–1FN), and CH_4–2-fluoronaphthalene (CH_4–2FN). Our objectives were to characterize the interaction potentials of the four systems in their electronic ground states, and to examine the changes in these potentials that occur when the substrates to which the weak bonds are formed are electronically excited. Ar and CH_4 were chosen as binding partners because of similarities in their properties. Both the van der Waals diameters and polarizabilities of Ar and CH_4 are nearly the same.[3] Thus, to the extent that the two binding partners can be represented as unstructured, spherically symmetric charge distributions, their interactions with the fluoronaphthalenes should be nearly the same. The excitation spectra of the Ar and cH_4 complexes should therefore be qualitatively similar.

In agreement with these expectations, the $S_1 \leftarrow S_0$ spectra of Ar–1/2FN and CH_4–1/2FN are qualitatively similar, at low resolution. However, their high resolution spectra are significantly different. The CH_4–1/2FN complexes exhibit origin bands that are each split into three distinct subbands with different intensities and separations of less than 1 cm^{-1}. No such splittings are observed in Ar–1/2FN. These differences may be traced to the anisotropy of the van der Waals interaction potential, and an incomplete averaging of this anisotropy by the rotational motion of the attached CH_4. Methane is, after all, not an unstructured atom but a structured molecule whose electronic distribution is *not* spherically symmetric. As will be shown, analyses of these results suggest that the formation of a weak bond between 1/2FN and the approaching CH_4 is perhaps better viewed from the perspective of a rapidly rotating spherical top interacting with an electron-rich ''surface'' whose properties may be modified by electronic excitation.

In what follows, we describe our experiments briefly and then present both the low and high resolution $S_1 \leftarrow S_0$ fluorescence excitation spectra of Ar–1/2FN and CH_4–1/2FN. We discuss the assignments of the observed bands and extract from these assignments the rotational constants of the connected vibronic levels in the two electronic states. We then determine the approximate geometries of the complexes from these constants and the polarizations of the observed bands. The results show that both binding partners are weakly attached to 1/2FN at a distance of ~3.5 Å above the aromatic plane. This distance decreases slightly on $S_1 \leftarrow S_0$ excitation. The results also show that both binding partners are displaced from the perpendicular inertial axes in both electronic states. We suggest that these transverse displace-

 0021-9606/95/102(16)/6432/12/$6.00

ments are a consequence of the vibrational averaging that occurs on the S_0 and S_1 surfaces of 1/2FN, surfaces that are significantly flatter along x and y than along z. Finally, we use a modified sum of atom–atom pair potentials to model these surfaces, and show that the observed splittings in the spectra of CH_4–1/2FN are consistent with a nearly freely rotating CH_4, only slightly perturbed by the presence of the nearby aromatic plane.

II. EXPERIMENT

1FN (2FN) was purchased from Aldrich (Custom Chemicals Laboratories) and used without further purification. In the low resolution experiments, the volatile 1FN or 2FN was minimally heated, seeded into 1–5 atm of various backing gases (described below), and expanded into a vacuum chamber through a 1 mm orifice pulsed valve (General Valve Series 9) operating at 10 Hz. The molecule was excited by a frequency-doubled dye laser pumped by a Nd^{3+}:YAG laser, also operating at 10 Hz. The spectral resolution of the dye laser is 0.5 cm^{-1}. The signal was detected by a photomultiplier tube (PMT) and processed by a boxcar integrator. A MASSCOMP MCS-561 data acquisition system was used to record the data. The spectra were not power normalized. Relative frequency calibration was performed using a solid étalon (FSR=1.0 cm^{-1}) at the fundamental of the dye.

High resolution data were obtained using a molecular beam laser spectrometer, described elsewhere.[4] The sample was heated to ~300 K, seeded in various backing gases (described below), expanded through a 100 μm quartz nozzle, skimmed once, and probed 15 cm downstream of the nozzle by a single frequency tunable ultraviolet (UV) laser. Fluorescence was collected using spatially selective optics, detected by a PMT and photon counting system, and processed by the MASSCOMP data acquisition system. Under the present operating conditions, the Doppler-limited spectral resolution was about 20 MHz in the UV. Relative frequency calibration was performed using a near-confocal interferometer having a mode-matched FSR of 299.7520±0.005 MHz at the fundamental of the dye. The absolute transition frequencies in both the low and high resolution spectra were determined by comparison to the I_2 absorption spectrum and are accurate to ~30 MHz.

Various expansion gases were used. Pure He backing gas was employed for the bare molecule experiments. Batch mixtures (by pressure) of Ar and CH_4 in He were used for the van der Waals complex experiments. Pure Ar backing gas also was employed for the Ar–2FN experiments at high resolution. In the mixed backing gas experiments the van der Waals complex intensity was optimized by varying the Ar and CH_4 percentage compositions with successive dilutions of He.

III. RESULTS

Shown in Fig. 1 are representative low resolution $S_1 \leftarrow S_0$ fluorescence excitation spectra of 1FN and its van der Waals complexes. Two prominent bands appear to the red of the electronic origin of bare 1FN in experiments carried out in an Ar/He carrier gas (trace B in Fig. 1). These appear at frequencies of −13.7 and −27.9±0.5 cm^{-1} with respect to the 0_0^0 band of 1FN. The first of these bands, at −13.7 cm^{-1}, is assigned to the single atom van der Waals complex Ar–1FN based on subsequent high resolution studies (*vide infra*). The second band, at $\Delta E = -27.9$ cm^{-1}, is believed to be due to Ar_2–1FN on the basis of the pressure and concentration dependence of its relative intensity, but this was not confirmed.

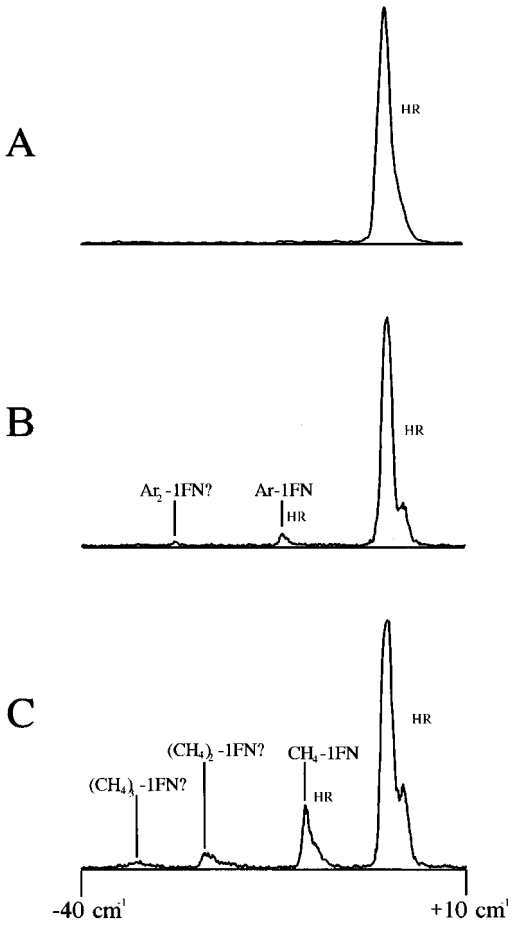

FIG. 1. Jet spectra of 1FN and its van der Waals complexes. All spectra span a frequency range of 50 cm^{-1}; the $S_1 \leftarrow S_0$ electronic origin of 1FN is at 0 cm^{-1} on the indicated frequency scale. Trace A was measured in pure He at ~5 atm. Trace B was measured in a ~1% Ar in He mixture, at a total pressure of ~9 atm. Trace C was measured in a ~1% CH_4 in He mixture, at a total pressure of ~9 atm. HR denotes bands examined at high resolution.

Trace C in Fig. 1 shows the corresponding spectrum of 1FN expanded in a mixture of CH_4/He. Three bands appear in this spectrum to the red of the 0_0^0 band of 1FN, at $\Delta E = -10.5$, −23.5, and −33.3±0.5 cm^{-1}. The first of these, at −10.5 cm^{-1}, is assigned to the single molecule van der Waals complex CH_4–1FN based on subsequent high resolution studies. The second and third bands are believed also to be due to CH_4–1FN complexes although this was not confirmed.

The low resolution spectra of 2FN expanded in pure He, an Ar/He mixture, and a CH_4/He mixture are qualitatively similar to the spectra in Fig. 1.[7] 2FN in Ar/He exhibits two red-shifted bands, at $\Delta E = -17.8$ and −35.1±0.5 cm^{-1}. The

TABLE I. Inertial parameters of the zero-point vibrational levels of the S_0 and S_1 electronic states of 2-fluoronaphthalene.

Parameter	S_0^a		S_1^a	
A(MHz)	2845.0(3)	[1920.6][b]	2764.0(3)	[1891.5]
B(MHz)	808.3(1)	[1122.2]	802.5(1)	[1102.1]
C(MHz)	629.6(1)	[708.5]	622.1(1)	[696.6]
κ	−0.8387(1)		−0.8316(1)	
ΔI(amu Å^2)	−0.18(2)		−0.26(2)	
υ_0 (cm^{-1})	31 800.08 (1) vac [31 866.508]			
Lines in fit	808			
σ (MHz)	4.3			

[a]2FN S_0-S_1 correlation matrix elements exceeding 0.950 are (C,C)=0.959.
[b]1FN values (Ref. 5).

first of these has been assigned to Ar–2FN. 2FN in CH_4/He exhibits three red-shifted bands, at $\Delta E=-18.8$, -28.3, and -40.4 ± 0.5 cm^{-1}. The first of these has been assigned to CH_4–2FN.

Prominent high frequency ''tails'' appear on the 0_0^0 bands of 1FN and 2FN recorded in the Ar/He and CH_4/He expansions. These are believed to be unresolved rotational contours that show up most prominently at the higher backing pressures employed to enhance complex formation. No He van der Waals complexes of 1/2FN were observed in any of the low resolution experiments.

The bare 1FN and 2FN molecules were both examined at high resolution. The results for 1FN were identical to those previously published.[5] The 0_0^0 band of the $S_1\leftarrow S_0$ transition of 1FN is an ab hybrid band, as expected for 1-substituted naphthalenes,[6] with 75% a character and 25% b character. (In naphthalene, the a axis is parallel to the long in-plane axis, x, and b is parallel to the short in-plane axis, y.) The corresponding band of 2FN is pure b type, as expected for 2-substituted naphthalenes.[6] It exhibits over 3500 lines at a rotational temperature of 12.5 K.[7] Fits of this band using rigid rotor Hamiltonians for the zero-point levels of both electronic states yielded the parameters listed in Table I. Like 1FN, 2FN is a rigid asymmetric top with small inertial defects ($\Delta I''=-0.18$ and $\Delta I'=-0.26$ amu Å^2). Thus, both molecules are planar in both electronic states.

Crucial to the success of similar high resolution experiments on the Ar and CH_4 van der Waals complexes of 1/2FN was the elimination of significant hot bands of the bare molecules, which also appear to the red of the 0_0^0 bands. Although they could not be completely removed, hot band contributions to the spectra could be minimized by careful adjustment of the backing pressures.

A representative high resolution spectrum of the most prominent Ar–1FN complex band, at 0_0^0 (1FN) -13.7 cm^{-1}, is shown in Fig. 2. This spectrum was recorded using a mixture of ~1% Ar in He at a total pressure of 110 psi. Like the bare molecule, Ar–1FN exhibits an ab-type spectrum, with 75% a character and 25% b character. Table II lists the inertial parameters obtained from a rigid rotor fit of this band. Comparison of these data with those for the bare molecule shows that, while rigid, Ar–1FN exhibits very large, negative inertial defects in both electronic states, $\Delta I''=-508$ and $\Delta I'=-518$ amu Å^2.

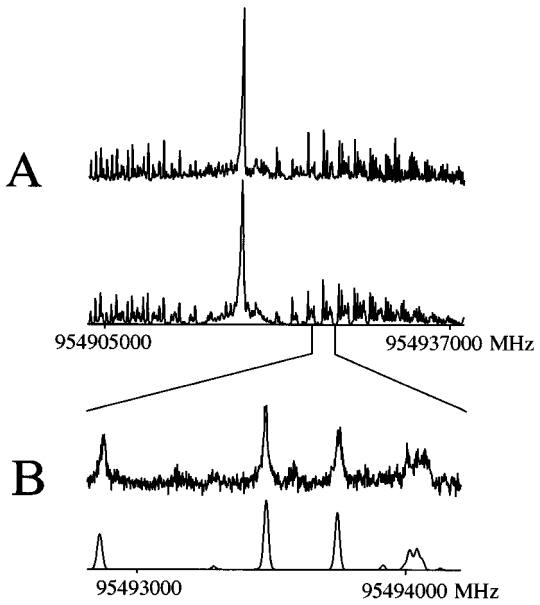

FIG. 2. Rotationally resolved fluorescence excitation spectrum of the (presumed) 0_0^0 band of the $S_1\leftarrow S_0$ transition in Ar–1FN ($p_0=110$ psi, 1% Ar in He). Panel A, which spans ~1 cm^{-1}, shows the overall experimental contour (top trace) and a theoretical simulation (bottom trace). The theoretical simulation required the convolution of 650 lines. Panel B, which spans ~0.03 cm^{-1}, shows a portion of the R branch at full experimental resolution (top trace) and a theoretical simulation (bottom trace); $T_r=2$ K.

The corresponding high resolution spectrum of the most prominent Ar–2FN complex band, at 0_0^0 (2FN) -17.8 cm^{-1}, is quite different in several respects.[7] First, the optimum conditions for the formation of this complex in the high resolution experiments were quite different. The most intense spectra were obtained in expansions of 2FN in pure Ar. Additionally, the spectrum is c-axis polarized, with an extremely congested Q branch. Finally, although the spectrum could be fit using rigid rotor Hamiltonians for both states, significantly better fits were obtained using the full Watson distortable rotor Hamiltonian.[8] Table III lists the inertial parameters derived from this fit. Like Ar–1FN, Ar–2FN has large, negative inertial defects, $\Delta I''=-342$ and $\Delta I'=-358$ amu Å^2.

Owing to the similarity of the low resolution spectra of the Ar and CH_4 complexes of 1/2FN, we anticipated that their high resolution spectra also would be qualitatively simi-

TABLE II. Inertial parameters of the zero-point vibrational levels of the S_0 and S_1 electronic states of Ar–1-fluoronaphthalene.

Parameter	S_0^a		S_1^a
A(MHz)	783.3(9)		781.0(8)
B(MHz)	713.6(2)		705.8(3)
C(MHz)	597.8(2)		598.1(1)
κ	0.249(4)		0.177(3)
ΔI(amu Å^2)	−507.9(8)		−518(8)
υ_0 (cm^{-1})	31 852.77 (1) vac		
Lines in fit	78		
σ (MHz)	5.7		

[a]S_0-S_1 correlation matrix elements exceeding 0.950 are $(C,C)=0.975$ and $(A,A)=0.962$.

TABLE III. Inertial parameters of the zero-point vibrational levels of the S_0 and S_1 electronic states of Ar–2 fluoronaphthalene.

Parameter	$S_0^{a,c}$	$S_1^{b,c}$
A(MHz)	905.5(3)	913.0(3)
B(MHz)	631.4(2)	618.7(2)
C(MHz)	496.9(4)	498.0(4)
κ	−0.342(2)	−0.423(2)
ΔI(amu Å^2)	−341.5(2)	−358.0(2)
D_k(MHz)	−0.13(2)	−0.06(2)
D_{jk}(MHz)	0.14(2)	0.07(2)
D_j(MHz)	−0.015(6)	−0.006(7)
d_k(MHz)	−0.06(2)	0.04(2)
d_j(MHz)	0.009(2)	−0.003(3)
H_k(MHz)	−0.000 6(3)	0.001 0(4)
H_{kj}(MHz)	0.000 9(7)	0.001 9(7)
H_{jk}(MHz)	−0.000 6(4)	−0.001 3(4)
H_j(MHz)	0.000 16(6)	0.000 28(7)
h_k(MHz)	0.000 8(4)	0.000 7(5)
h_{jk}(MHz)	−0.000 4(3)	0.000 1(3)
h_j(MHz)	−0.000 07(3)	−0.000 14(3)
v_0 (cm^{-1})	31 782.29 (2) (vac)	
Lines in fit	218	
σ (MHz)	3.8	

[a]S_0-S_0 correlation matrix elements exceeding 0.950 are $(H_k,H_{kj})=-0.967$.
[b]S_1-S_1 correlation matrix elements exceeding 0.950 are $(H_k,H_{kj})=-0.982$, $(H_{kj},h_k)=-0.972$, $(H_{kj},H_{jk})=-0.958$, and $(H_k,h_k)=0.956$.
[c]S_0-S_1 correlation matrix elements exceeding 0.950 are $(h_k,h_k)=0.979$, $(H_k,H_k)=0.960$, $(H_{kj},H_{kj})=0.952$, and $(h_k,H_{kj})=0.953$.

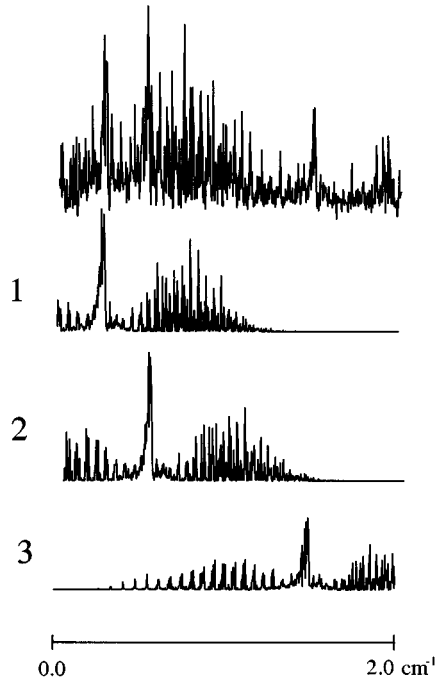

FIG. 3. Rotationally resolved fluorescence excitation spectrum of the (presumed) 0_0^0 band of the $S_1\leftarrow S_0$ transition in CH_4–1FN [at 0_0^0 (1FN)−10.5 cm^{-1}], showing the splitting of the band into three component subbands 1, 2, and 3. Computer simulations of the three component subbands are shown in the traces below. $T_r=2.5$ K. In the experiment, 1FN was seeded into a backing gas mixture of ~1% CH_4 in He at 120 psi.

lar. This is not the case. *At high resolution, the CH_4–1/2FN spectra exhibit three closely spaced subbands, instead of the single vibronic bands observed in the high resolution spectra of Ar–1/2FN.* A representative high resolution spectrum of the most prominent CH_4–1FN complex band, at 0_0^0 (1FN) −10.5 cm^{-1}, is shown in Fig. 3. Three parallel-type Q branches are readily apparent in this spectrum. The three Q branches lie within a 2 cm^{-1} range; the separations of the subband origins are 0.229 and 0.932±0.002 cm^{-1}. Careful studies of the backing pressure dependence of the relative intensities of the three subbands showed, further, that these intensities are pressure independent, having values of 2:2:1, ±10%.

Despite the high density of lines, fits of each subband in the $S_1\leftarrow S_0$ spectrum of CH_4–1FN proved to be relatively straightforward. A representative example is shown in Fig. 4. The presence of the parallel-type Q branches made possible spectral assignments to the recognizable patterns that arise from a-type selection rules. Later in the analysis, dimmer b-type lines were distinguished. The final simulation of the entire spectrum (Fig. 4) assumed a rotational temperature of 2.5 K (at a total backing gas pressure of 120 psi, 1% CH_4 in He), a relative intensity ratio 2:2:1, 75% a character and 25% b character for each subband, and a Voigt lineshape profile, with a 1.4 MHz Lorentzian component[5] and a 26 MHz Doppler component for individual lines in each subband.

Summarized in Table IV are the inertial parameters that were derived from rigid rotor fits of subbands 1, 2, and 3. Each of the six different vibronic levels exhibits significantly different rotational constants. This shows that all levels are unique. None of the three vibronic bands appear to share a common level, in either electronic state. But all levels are the vibronic levels of a rigid asymmetric top. Additionally, all levels exhibit large, negative inertial defects, ranging from $\Delta I''=-355$ to -370 amu Å^2 in the S_0 state and from $\Delta I'=-344$ to -368 amu Å^2 in the S_1 state.

Similar results were obtained for the methane van der Waals complex of 2-fluoronaphthalene.[7] Here, however, the analysis was significantly more difficult. The most prominent CH_4–2FN complex band at 0_0^0 (2FN) −18.8 cm^{-1} also exhibits three underlying subbands (1, 2, and 3) separated by only 0.14 and 0.52±0.01 cm^{-1}. The (pressure-independent) relative intensities of the three bands in CH_4–2FN also are the same as in CH_4–1FN, 2:2:1,±10%. The signal level in CH_4–2FN is, however, significantly lower than that in CH_4–1FN, making hot band interference a larger problem in the analysis. Additionally each subband is 100% b-type polarized, creating significantly larger overlap of the three, since the K_a components shift linearly with A (rather than quadratically with ΔA). The separation of the three subbands is very nearly an integral multiple of A. The analysis was aided by recording several spectra at extremely high backing pressures, so that only the transitions originating in $K_a=0$ and 1 contributed significant intensity. Finally, given the distortable rotor character of the 0_0^0 band of the Ar–2FN complex, several fits of the two brighter subbands of CH_4–2FN using the Watson Hamiltonian[8] were attempted. Significant differences in the resulting standard deviations of the fits were not obtained, perhaps because of the smaller numbers of unambiguously assigned lines. Only rigid rotor models for

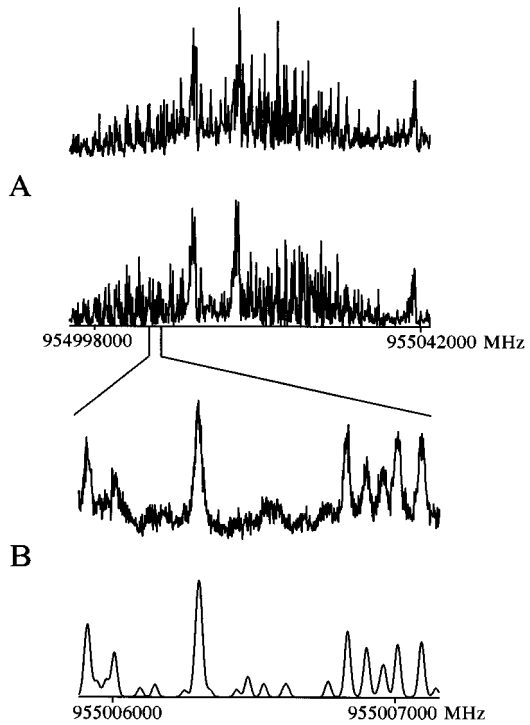

FIG. 4. Fits of the fully-resolved $S_1 \leftarrow S_0$ spectrum of CH_4–1FN. Panel A shows the full experimental spectrum (top trace) and a theoretical simulation (bottom trace). The simulation required 3006 calculated lines. Panel B shows a portion of the experimental spectrum (top trace) and a corresponding theoretical simulation (bottom trace) at full experimental resolution. Panel B contains significant transition intensity from both subbands 1 and 2. The bright lines left of center in panel B are $K_a=0$, 1, and 2 lines of the $J=2$ family of subband 1. Careful examination of panel B shows the presence of additional lines and an increased background in the experimental trace not accounted for by the simulations. These are due to hot bands of the bare molecule.

TABLE IV. Inertial parameters of the six zero-point vibrational levels observed in the fully resolved $S_1 \leftarrow S_0$ fluorescence excitation spectrum of CH_4–1-fluoronaphthalene.

	CH_4–1FN subbands		
Parameter	$1(E \leftrightarrow E)$[a]	$2(F \leftrightarrow F)$[b]	$3(A \leftrightarrow A)$[c]
A''(MHz)	1 131.9(4)	1 125.5(2)	1 130.1(3)
B''(MHz)	797.0(2)	795.4(1)	797.9(1)
C''(MHz)	707.8(1)	707.5(1)	696.7(1)
κ''	−0.579 1(1)	−0.579 6(1)	−0.532 7(1)
$\Delta I''$(amu Å^2)	−366.5(2)	−369.9(2)	−355.1(1)
A'(MHz)	1 124.3(4)	1 119.6(2)	1 122.2(3)
B'(MHz)	788.2(2)	786.6(1)	788.6(1)
C'(MHz)	696.6(1)	696.6(1)	676.7(1)
κ'	−0.571 6(1)	−0.574 5(1)	−0.497 5(1)
$\Delta I'$(amu Å^2)	−365.2(2)	−367.9(1)	−344.3(1)
ΔE (cm^{-1})	−10.748(2)	−10.518(2)	−9.586(2)
v_0 (cm^{-1})	31 855.761(2)	31 855.990(2)	31 856.922(2)
Lines in fit	135	112	124
σ(MHz)	4.4	6.5	7.7

[a]S_0-S_1 correlation matrix elements exceeding 0.950 are $(A,A)=0.997$, $(C,C)=0.980$, and $(B,B)=0.971$.
[b]S_0-S_1 correlation matrix elements exceeding 0.950 are $(A,A)=0.993$ and $(B,B)=0.962$.
[c]S_0-S_1 correlation matrix elements exceeding 0.950 are $(A,A)=0.997$, $(B,B)=0.962$, and $(C,C)=0.961$.

TABLE V. Inertial parameters of the six zero-point vibrational levels observed in the fully resolved $S_1 \leftarrow S_0$ fluorescence excitation spectrum of CH_4–2-fluoronaphthalene.

	CH_4–2FN subbands		
Parameter	$1(E \leftrightarrow E)$[a]	$2(F \leftrightarrow F)$[b]	$3(A \leftrightarrow A)$[c]
A''(MHz)	1 400.8(1)	1 385.3(2)	1 395(2)
B''(MHz)	627.9(3)	631.9(1)	623.2(5)
C''(MHz)	619.2(2)	620.0(1)	620.6(4)
κ''	−0.978(1)	−0.969(1)	−0.993(1)
$\Delta I''$ (amu Å^2)	−349.5(2)	−349.5(1)	−358.9(8)
A'(MHz)	1 385.5(1)	1 371.9(2)	1 386(1)
B'(MHz)	623.9(9)	629.7(1)	622.7(5)
C'(MHz)	615(1)	615.8(1)	615.5(3)
κ'	−0.978(1)	−0.965(1)	−0.981(1)
$\Delta I'$(amu Å^2)	−353.4(1)	−351.2(1)	−355.1(7)
ΔE(cm^{-1})	−18.98(1)	−18.84(1)	−18.32(1)
v_0(cm^{-1})	31 781.10(1)	31 781.24(1)	31 781.76(1)
Lines in fit	93	106	18
σ(MHz)	3.8	10.9	11.9

[a]Correlation matrix elements exceeding 0.950 are $(A,A)=0.951$ (S_0-S_0) and $(B,C)=-0.981(S_0-S_1)$.
[b]Correlation matrix elements exceeding 0.950 are $(A,A)=0.967(S_0-S_1)$.
[c]Correlation matrix elements exceeding 0.950 are $(B,C)=0.960$ (S_0-S_0), $(A,A)=0.987$ (S_0,S_1), $(B,C)=0.954$ (S_0,S_1), and $(B,B)=0.951$ (S_0-S_1).

all six vibronic levels were used in the final analysis. The resulting inertial parameters are listed in Table V.

Examination of the data in Table V shows that the differences in the rotational constants of the three S_0 vibronic levels and the three S_1 vibronic levels of CH_4–2FN are significantly smaller than in the case of CH_4–1FN. However, all vibronic levels are still unique. Like CH_4–1FN, the vibronic levels of CH_4–2FN also exhibit large, negative ΔI values, lying between −350 and −359 amu Å^2 in the S_0 state and between −351 and −355 amu Å^2 in the S_1 state.

IV. DISCUSSION

A. Approximate complex geometries

A common property of the Ar and CH_4 complexes of 1/2FN is that they all exhibit large, negative inertial defects in their S_0 and S_1 electronic states. Thus, conclusions regarding their approximate geometries can be reached using simple inertial arguments.[9] In the principal axis system, abc, of the bare molecule, the inertia tensor has the form

$$I=\begin{pmatrix} I_a & & \\ & I_b & \\ & & I_c \end{pmatrix}. \tag{1}$$

If the molecule is planar, then $I_c=I_a+I_b$. As we have seen, both 1FN and 2FN conform approximately to this equation; with $a=x$, $b=y$, and $c=z$; z being perpendicular to the molecular plane. Adding a mass m at the point (x,y,z) converts Eq. (1) to

$$I=\begin{Bmatrix} [I_a+\mu(y^2+z^2)] & -\mu xy & -\mu zx \\ -\mu xy & [I_b+\mu(z^2+x^2)] & -\mu yz \\ -\mu zx & -\mu yz & [I_c+\mu(x^2+y^2)] \end{Bmatrix}, \tag{2}$$

where $\mu=mM/(m+M)$ and M is the mass of 1/2FN. However, in the special case where the attached mass is located along one of the principal axes of the bare molecule (e.g., $c=z$), then Eq. (2) takes the special form

$$I=\begin{bmatrix} (I_a+\mu z^2) & 0 & 0 \\ 0 & (I_b+\mu z^2) & 0 \\ 0 & 0 & I_c \end{bmatrix} \tag{3}$$

since $|x|=|y|=0$. Equation (3) shows, then, that if the attached atom or molecule lies along an inertial axis of the bare molecule, one of the principal moments of inertia is unchanged on complex formation (here, I_c), and the remaining two moments change by the same amount (here, μz^2).

The measured rotational constants are, of course, inversely related to the principal moments of inertia. Listed in Table VI are the inertial moments I_g $(g=a,b,c)$ derived from the reciprocal rotational constants of the ground electronic states of 1FN and 2FN and the incremental changes in these constants ΔI_g that occur on complex formation. Examination of the data in this table shows immediately that $I_c \approx I_a+I_b$ in both 1FN and 2FN, as expected for a planar molecule. Further, the CH_4 complexes of both 1FN and 2FN conform, at least approximately, to Eq. (3). Thus, attaching a CH_4 to the planar 1FN results in positive ΔI_a and ΔI_b values that are approximately equal $(\approx \mu z^2)$ and a near-zero value of ΔI_c. The corresponding values of $\Delta I_a, \Delta I_b$, and ΔI_c for CH_4–2FN are approximately the same as those for CH_4–1FN, although ΔI_c is significantly different from zero. Thus, we conclude that in both CH_4–1FN and CH_4–2FN, the methane molecule lies along (or nearly along) the c axis of the bare molecule, above (or below) the 1/2FN plane. This conclusion is consistent with the findings that the inertial defects of CH_4–1/2FN are both large and negative, these being indicative of nonplanar structures.[9]

The 0_0^0 bands of the $S_1 \leftarrow S_0$ transitions of both 1FN and 2FN are both in-plane polarized, 75:25% $a:b$ for 1FN and 100% b for 2FN. The corresponding transitions of both CH_4 complexes are similarly polarized, despite the presence of the methane molecule above the fluoronaphthalene plane. Clearly, the weak van der Waals interaction between the two binding partners has little or no effect on the oscillating charge distribution that is produced by $S_1 \leftarrow S_0$ excitation of the bare molecule.

TABLE VI. Inertial moments (in units of 10^2 amu Å^2) of S_0 1FN and 2FN and their van der Waals complexes.

	I_g	$\Delta I_g(CH_4)$[a]	$\Delta I_g(Ar)$[b]
1FN/*A*	2.63[c]	1.83	3.82
1FN/*B*	4.50[c]	1.84	2.58
1FN/*C*	7.13[c]	0.01	1.32
2FN/*A*	1.77	1.83	3.81
2FN/*B*	6.25	1.80	1.75 (3.92)[d]
2FN/*C*	8.03	0.14	2.14 (−0.02)[d]

[a]$\Delta I_g=[I_g(CH_4\text{–}1/2FN)-I_g(1/2FN)];g=a,b,c$. The I_g values for CH_4–1/2FN are the average S_0 values of subbands 1, 2, and 3.
[b]$\Delta I_g=[I_g(Ar\text{–}1/2FN)-I_g(1/2FN)];g=a,b,c$.
[c]Reference 5.
[d]With $x=a, y=c$, and $z=b$.

Ar–1FN also conforms, at least approximately, to the expectations of Eq. (3). As in the case of CH_4–1FN, the largest changes are ΔI_a and ΔI_b (cf. Table VI). These are larger in the case of Ar–1FN because of the larger mass of argon. However, now $\Delta I_a > \Delta I_b$, and $\Delta I_c \neq 0$. This suggests that the argon atom in Ar–1FN is displaced slightly from the c axis of 1FN. Further, since $\Delta I_a > \Delta I_b$, the moments I_a and I_b of Ar–1FN are now more nearly equal, rather than I_b and I_c. Nonetheless, the polarization of the 0_0^0 band of Ar–1FN is the same as that of the bare molecule. Thus, we can safely conclude that the argon atom in Ar–1FN lies above the 1FN plane and only weakly interacts with the S_0 and S_1 charge distributions.

Ar–2FN is different. Its ΔI_g values are different (cf. Table VI) and the 0_0^0 band of its $S_1 \leftarrow S_0$ transition is c-axis polarized, unlike the bare molecule. But these differences are only apparent, not real. This is because the c axis of Ar–2FN corresponds to the b axis of 2FN. The added mass produces a reordering of the moments in the molecular frame. (Unlike 1FN, bare 2FN has more nearly equal values of I_b and I_c.) Thus, with $a=x$, $c=y$, and $b=z$ (cf. Table VI), we again find that $\Delta I_a \approx \Delta I_b$, and $\Delta I_c \approx 0$. ($\Delta I''=-774$ amu Å^2 in this coordinate system.) So, as in the case of Ar–1FN, we conclude that the argon atom in Ar–2FN lies above the 2FN plane and has little or no effect on the orientation of the $S_1 \leftarrow S_0$ transition moment.

Since $\Delta I_c \approx 0$ in all four complexes, this argument can be extended to obtain estimates of the out-of-plane displacements of the binding partners above (or below) the 1/2FN planes from the observed ΔI_a $(\approx \Delta I_b)$ values $(\approx \mu z^2)$. Indeed, this is the "traditional" approach used in studies of the rotationally resolved electronic spectra of van der Waals complexes of aromatic molecules.[10] However, this approach neglects the fact that, in most cases (cf. Table VI), ΔI_c is not rigorously zero, nor is ΔI_a rigorously equal to ΔI_b. While small, these deviations are significant since they are intimately related to the important issues of vibrational averaging and the anisotropy of the van der Waals potential. Therefore, we shall not take this approach here.

B. The Ar complexes: A more detailed view

More meaningful values of the positions of the argon atoms in Ar–1FN and Ar–2FN can be obtained using Kraitchman's equations.[11] These equations are analytical solutions of Eq. (2) from which values of the center-of-mass

TABLE VII. Center-of-mass coordinates of argon in the S_0 and S_1 electronic states of Ar–1FN and Ar–2FN.[a,b]

	Ar–1FN	Ar–2FN
$\|x\|$, Å (S_0)	0.132 (9)	0.232 (11)
$\|y\|$, Å (S_0)	0.383 (11)	0.513 (15)
$\|z\|$, Å (S_0)	3.482 (4)	3.456 (4)
$\|x\|$, Å (S_1)	0.207 (5)	0.412 (9)
$\|y\|$, Å (S_1)	0.483 (7)	0.513 (18)
$\|z\|$, Å (S_1)	3.408 (3)	3.435 (3)

[a]In the principal axis frames of 1FN and 2FN.
[b]Errors in the coordinates were determined by propagating the errors in the measured rotational constants through Kraitchman's equations.

(COM) coordinates of the attached mass *m* can be determined. The accuracy of this procedure depends on the reliability of the assumption that the attached mass does not change the inertial contributions of the mass centers that make up the *original* frame. This seems a reasonably safe assumption for Ar–1/2FN. Attaching an argon atom to either 1FN or 2FN via a weak out-of-plane van der Waals "bond" should have little or no effect on the significantly stronger covalent bonds of the two substrates.

To apply Kraitchman's equations to this problem, we assumed that 1/2FN was a complex with a hypothetical argon atom of zero mass. Then, we determined the COM coordinates of the argon atom from the changes in the rotational constants that are observed when the hypothetical atom is replaced by a *real* argon atom in Ar–1/2FN, in both electronic states. The results are listed in Table VII. The out-of-plane coordinates $|z|$ are similar in both complexes, 3.48 and 3.46 Å in the ground states of Ar–1FN and Ar–2FN, respectively. The $|z|$ coordinates decrease on electronic excitation, to 3.41 and 3.44 Å, respectively. These decreases are consistent with the observation that the 0_0^0 bands of the complexes are both red shifted relative to the 0_0^0 bands of the bare molecules. The van der Waals bonds are stronger in the S_1 states of Ar–1/2FN. But the decrease in $|z|$ for Ar–1FN (0.07 Å) is significantly larger than that for Ar–2FN (0.02 Å). This result is apparently inconsistent with the relative magnitudes of the shifts, -10.5 and -17.8 cm^{-1} in Ar–1FN and Ar–2FN, respectively.

As surmised earlier, the values of $|x|$ and $|y|$ in both states of Ar–1/2FN are small, but *not zero*. For example, the argon atom in S_0 Ar–1FN has $|x|=0.13$ and $|y|=0.38$ Å (cf. Table VII). These nonzero values could be simple, static displacements of the attached rare gas atom from the COM, owing to the noncylindrically symmetric charge distributions of 1/2FN. But the measured coordinates also could be subject to significant vibrational averaging. Properly interpreted, they should be regarded as root-mean-square (rms) displacements averaged over the complete vibrational wave functions of the complexes (e.g., $|x|=1/\langle 1/x^2\rangle^{1/2}$).[12] Thus, we do not know, *a priori*, the extent to which the measured values of $|x|$, $|y|$, and $|z|$ reflect *static* displacements of the argon atoms from the COM, and the extent to which these values reflect *dynamic* displacements of the argon atoms from their equilibrium positions. Unfortunately, the two effects interfere with each other.

Some insight into the relative importance of these two effects is provided by the recent calculations of Mandziuk and Bačić[13] on argon–naphthalene (Ar–N). These authors constructed an intermolecular PES using simple atom–atom pair potentials. They then used a 3D discrete variable representation to determine the eigenfunctions and eigenvalues of the van der Waals vibrational modes of Ar–N. The calculated S_0 PES has two equivalent minima at $\{x,y,z\}_{min}=\{\pm 0.41, 0.0, 3.47$ Å$\}$. The depth of the minima is -383 cm^{-1}, the barrier separating them is only ~ 0.3 cm^{-1}. The corresponding parameters of S_1 Ar–N are $\{x,y,z\}_{min}=\{\pm 0.47, 0.0, 3.44$ Å$\}$, -399 cm^{-1}, and ~ 0.5 cm^{-1}, respectively. Both PES's are very shallow along x; they rise to only ~ 75 cm^{-1} at $x=\pm 2$ Å. The surfaces are only slightly steeper along y. The two lowest bending frequencies are at 5.5 and 16.4 cm^{-1}. Thus, the corresponding zero-point levels lie above the barrier along x and the Ar atom exhibits large amplitude motions in both in-plane directions, in both electronic states. The calculated S_0 rms displacements are $\Delta x=0.44$ and $\Delta y=0.34$ Å. The first excited stretching mode in S_0 Ar–N lies at 40.6 cm^{-1}. So, the PES is considerably steeper along the out-of-plane coordinate, z. As a result, the motion of the Ar atom is significantly quenched in this direction, in both electronic states. The calculated S_0 rms displacement is $\Delta z=0.12$ Å.

We believe that a similar situation exists in both the S_0 and S_1 states of Ar–1/2FN. Thus, we interpret the measured $|x|$ and $|y|$ values as "dynamic" displacements, and the measured $|z|$ value as a "static" displacement. To make a more meaningful comparison of experiment with theory, *ab initio* calculations were performed on the ground electronic states of N, 1FN, and 2FN at the HF/6-31G* level.[14] Optimized geometries with respect to both in-plane and out-of-plane distortions were determined for each molecule. (All are planar at this level of theory.) Then, using the calculated COM's of each molecule, and the relative orientations of their principal axes, the measured COM coordinates of the argon atoms in Ar–1FN and Ar–2FN were mapped onto the naphthalene coordinate system. The resulting values, $|x|_N$, etc., are listed in Table VIII. Also listed in this table are the rms displacements, Δx, etc., and the vibrationally averaged values of z, $\langle z\rangle$, in the zero-point vibrational levels of S_0 and S_1 Ar–N calculated by Mandziuk and Bačić.[13]

Comparing these results, we see that there is reasonable agreement between the calculated $\langle z\rangle$ values of S_0 and S_1 Ar–N and the measured $|z|_N$ values of S_0 and S_1 Ar–1/2FN. Both are observed to decrease on electronic excitation. The calculated red shift,[13] -16 cm^{-1}, also is in qualitative accord with the measured values for Ar–1/2FN, -10.5 and -17.8 cm^{-1}, respectively. (The experimental value in Ar–N is -14.0 cm^{-1}.[15]) But there are significant differences between the theoretical results for Ar–N and the experimental results for Ar–1/2FN. The value of $|x|_N$ in S_0 Ar–1FN is smaller than Δx in S_0 Ar–N, whereas the value of $|y|_N$ in S_0 Ar–1FN is larger than Δy in S_0 Ar–N. Now, replacement of a hydrogen atom in the 1-position of N by a fluorine atom in 1FN moves the COM by ~ 0.1 Å in the x direction and ~ 0.3

TABLE VIII. Vibrationally averaged argon atom coordinates in the S_0 and S_1 electronic states of Ar–N, Ar–1FN, and Ar–2FN.

	Ar–N[a]	Ar–1FN[b]	Ar–2FN[b]
$\|x\|_N$, Å (S_0)	0.437	0.106	0.508
$\|y\|_N$, Å (S_0)	0.335	0.728	0.752
$\|z\|_N$, Å (S_0)	3.506	3.482	3.456
$\|x\|_N$, Å (S_1)	0.440	0.154	0.686
$\|y\|_N$, Å (S_1)	0.328	0.844	0.779
$\|z\|_N$, Å (S_1)	3.475	3.408	3.435

[a]Reference 13. Here, the listed coordinates $|x|_N$ and $|y|_N$ for Ar–N are the calculated root mean square displacements Δx and Δy; $|z|_N$ is the vibrationally averaged value $\langle z \rangle$. Δz is 0.119Å in S_0 Ar–N and 0.117 Å in S_1 Ar–N.

[b]Experimental coordinates, referred to the principle axis system of naphthalene (see text).

Å in the y direction. The latter displacement is, we believe, principally responsible for the difference between $|y|_N$ and Δy. But $|x|_N$ is *less* than Δx. This comparison suggests, then, that 1-fluoro substitution significantly reduces the large amplitude motion of the Ar atom along the x axis of 1FN while having relatively little effect on the amplitude of its motion along y. A similar situation exists in the S_1 state of Ar–1FN. But the situation is different in both states of Ar–2FN. Here, the values of $|x|_N$ and $|y|_N$ are both larger than Δx and Δy in Ar–N. The values of $|y|_N$ are substantially larger than Δy. Replacement of a hydrogen atom in the 2-position of N by a fluorine atom in 2FN moves the COM by ~0.4 Å in the x direction and only ~0.2 Å in the y direction. Thus, it appears that the argon atom in Ar–2FN executes large amplitude motion in *both* transverse directions, especially along y. This may explain why distortion terms were required to fit the $S_1 \leftarrow S_0$ spectrum of Ar–2FN, and why Ar–2FN exhibits a larger red shift than Ar–1FN. $|x|_N$ increases significantly on electronic excitation of Ar–2FN.

C. The CH_4 complexes: A more detailed view

Methane is a more sensitive probe of the anisotropy of the intermolecular PES because of its rotational motion. Recall that the 0_0^0 bands in the $S_1 \leftarrow S_0$ spectra of CH_4–1/2FN are each split into three subbands. Similar splittings have been observed in D_2-*t*-stilbene,[16] H_2/D_2–aniline and CH_4–aniline,[17] and $CH_4/CH_3D/CH_2D_2$–perylene,[18] although the resulting subbands have not been rotationally resolved. One possible explanation for these splittings is that there are chemically distinct isomers, three in the case of CH_4–1/2FN. One can easily imagine configurations with one, two, and three CH bonds pointing down towards the "surface" plane. Distinguishable isomers of this sort could have different rotational constants. They also might have distinguishable $S_1 \leftarrow S_0$ spectra if their zero-point energies are sufficiently different. But CH_4 has a large rotational constant, $B = 5.2$ cm^{-1}.[19] Thus, the rotational energy level spacings in the free, gas phase molecule are comparable to the intermolecular vibrational frequencies of CH_4–1/2FN. It is therefore reasonable to suppose that the vibrating methane molecule in CH_4–1/2FN also might be free to rotate. In that event, the observed splittings can be attributed to differences in the degrees to which the rotational motion of the attached CH_4 averages out anisotropies in the van der Waals potential.

If rotational motion is permitted in the van der Waals "well," then nuclear spin statistics become important. The rotational wave functions of an undistorted CH_4 must belong to one of the irreducible representations of T_d; A, E, or $F(T)$. The three different types of rotational levels have different statistical weights. As shown by Wilson,[20] the species of the nuclear spin functions of a tetrahedral CH_4 are $5A+E+3F$. For the A rotational levels ($J=0,3,...$), we have to use a spin function of species A; the total (rotational $\otimes$ nuclear) statistical weight is $5(2J+1)$. For the E rotational levels ($J=2,4,\ldots$), we have to use a spin function of species E; since $E \otimes E$ gives two functions of species A, the total statistical weight is $2(2J+1)$. For the F rotational levels ($J=1,2,\ldots$), we have to use a spin function of species F; since $F \otimes F$ gives one function of species A, the total statistical weight is $3(2J+1)$. Now, our experiments were done in the collision-free environment of a molecular beam. Under these conditions, it is reasonable to assume that the CH_4 molecules are in their lowest allowed quantum states, $J=0,1$, and 2. Owing to the unique spin symmetries of these levels, all will be populated, even at 0 K. And their relative populations should scale according to their *total* statistical weights. For $J=0$, this weight is 5. For $J=1$, this weight is 9. And for $J=2$, this weight is 10; we neglect the contribution of the F levels since they will relax to $J=1$. *Importantly, these statistical weights are the same (within experimental error) as the relative intensities of the three closely spaced vibronic bands in both CH_4–1FN and CH_4–2FN, 1:2:2.* Therefore, we attribute the splittings observed in the $S_1 \leftarrow S_0$ spectra of CH_4–1/2FN to the rotational motion of the attached CH_4. We assign the three bands to three superimposed transitions of CH_4–1FN (or CH_4–2FN). The three bands may be distinguished by the rotational (and nuclear spin) quantum numbers of the attached methane. The two strong bands are the $E \leftrightarrow E(J=2)$ and $F \leftrightarrow F(J=1)$ transitions; the weak band is the $A \leftrightarrow A(J=0)$ transition. Similar effects have been observed in CH_4–HCl,[21] CH_4–H_2O,[22] and Ar–SiH_4.[23]

Since the three bands of CH_4–1/2FN occur at slightly different energies, and yield on analysis rotational constants that are slightly different, it is necessary to postulate that there are slight differences in the way that the $J=0$, 1, and 2 methanes "bind" to the substrate 1FN and 2FN molecules. Stated differently, it must be that the nature of the "(ro)vibrational averaging" in the three different rotational states of methane is different. Since the rotational wave functions of $J=0$, 1, and 2 CH_4 have different symmetries, this is not a surprising result. A preferential adsorption of different spin states of the same molecule on a "real" surface has been observed.[24]

Detailed studies of this effect should provide valuable new information about the subtle anisotropies of gas–surface potentials. But such studies will require significant computational effort. So, here we take a somewhat more intuitive approach. Our objective is to explain the patterns of the observed transitions, rationalize the magnitudes of the observed

TABLE IX. Center-of-mass coordinates of methane in the S_0 and S_1 electronic states of CH_4–1FN.[a,b]

	Band 1 ($E\leftrightarrow E$)	Band 2 ($F\leftrightarrow F$)	Band 3 ($A\leftrightarrow A$)
$\|x\|$, Å (S_0)	0.15 (2)	0.06 (4)	0.47 (1)
$\|y\|$, Å (S_0)	0.06 (2)	0.14 (1)	0.39 (1)
$\|z\|$, Å (S_0)	3.564(1)	3.586(1)	3.571(1)
$\|x\|$, Å (S_1)	0.08 (4)	0.08 (3)	0.65 (1)
$\|y\|$, Å (S_1)	0.06 (2)	0.05 (2)	0.54 (1)
$\|z\|$, Å (S_1)	3.554(1)	3.570(1)	3.561(1)

[a]In the principal axis frame of 1FN.
[b]Errors in the coordinates were determined by propagating the errors in the measured rotational constants through Kraitchman's equations.

splittings, and gain some understanding about how these features can be related to the interaction potentials that govern them.

The perspective we take is that of a weakly bound, rotating CH_4 that is slightly perturbed by its interaction with the 1FN and 2FN surfaces. To develop this perspective, we first treat the CH_4 as a structureless particle, replacing the five mass centers with a single point mass. We then use Kraitchman's equations to determine the vibrationally averaged COM positions of this hypothetical particle in the S_0 and S_1 states of CH_4–1/2FN. The results are listed in Tables IX and X. Three sets of values are reported for each complex, one set for each of the three subbands (1, 2, and 3). Examining these results, we see that, in general, the derived values of $|x|$ and $|y|$ are slightly different from zero, as in the case of Ar–1/2FN. The ground state $|z|$ values are comparable to, but somewhat larger than those of the Ar complexes, a reasonable result given the larger van der Waals diameter of CH_4 (3.82 vs 3.41 Å).[3] And, again, the $|z|$ values decrease slightly on $S_1\leftarrow S_0$ excitation. We conclude from these observations, then, that the PES's of CH_4–1/2FN are qualitatively similar to those of Ar–1/2FN, relatively flat along x and y and steep along z, in both electronic states. The small differences in the measured coordinates of the three subbands (cf. Tables IX and X) may be attributed to differences in the degrees of rovibrational averaging experienced by the different rotational states of the attached CH_4.

TABLE X. Center-of-mass coordinates of methane in the S_0 and S_1 electronic states of CH_4–2FN.[a,b]

	Band 1 ($E\leftrightarrow E$)	Band 2 ($F\leftrightarrow F$)	Band 3 ($A\leftrightarrow A$)
$\|x\|$, Å (S_0)	0.49 (1)	0.07 (4)	0.56 (2)
$\|y\|$, Å (S_0)	0.10 (1)	0.12 (1)	0.06 (1)
$\|z\|$, Å (S_0)	3.574(1)	3.597(1)	3.593(1)
$\|x\|$, Å (S_1)	0.43 (3)	0.33 (1)	0.47 (2)
$\|y\|$, Å (S_1)	0.11 (1)	0.17 (1)	0.09 (1)
$\|z\|$, Å (S_1)	3.557(2)	3.573(1)	3.558(3)

[a]In the principal axis frame of 2FN.
[b]Errors in the coordinates were determined by propagating the errors in the measured rotational constants through Kraitchman's equations.

To model this motion, we position the CH_4 at $(x,y,z)=(0.0, 0.0, 3.5$ Å), above the plane of the uncomplexed 1FN or 2FN at a distance $R(=z)$ that is approximately the same as that derived from the Kraitchman analysis. Then we compute the resulting energy levels of the rotating CH_4. The relevant Hamiltonian is

$$\hat{H}=\frac{\hat{p}^2}{2I}+\hat{V}(\theta,\phi,\chi), \tag{4}$$

where $\hat{p}^2/2I$ is the rotational kinetic energy operator for the CH_4 rotor with matrix elements $BJ(J+1)$, $\hat{V}(\theta,\phi,\chi)$ is the potential energy operator over the angular degrees of freedom at fixed R, and (θ,ϕ,χ) are the standard Euler angles. The basis set chosen is the set of symmetric top functions $|JKM\rangle$ that span the full angular space. In the Euler angle representation, this basis has the form

$$|JKM\rangle=\left(\frac{2J+1}{8\pi}\right)^{1/2}D_{JKM}(\theta)e^{iK\phi}e^{iM\chi}, \tag{5}$$

where the D_{JK} are related to elements of the well-known rotation matrices.[25] The matrix elements of $\hat{V}$ in this basis are (at constant R),

$$\langle JKM|\hat{V}(\theta,\phi,\chi)|J'K'M'\rangle = \int_0^{2\pi}\int_0^{2\pi}\int_0^{\pi}\Psi_{JKM}\hat{V}(\theta,\phi,\chi) \times\Psi_{J'K'M'}\sin\theta\, d\theta\, d\phi\, d\chi. \tag{6}$$

In what follows, we perform this integration numerically using a modified trapezoidal rule scheme.[26] We employ a $(60\times60\times60)$ grid that samples the spherical integration space (θ,ϕ,χ). Eigenvalues and eigenfunctions were obtained by diagonalizing Eq. (4) using a basis set of 35 wave functions.

The key issue in this calculation is how to incorporate the structure of CH_4. A rotating CH_4 will average out much of the anisotropy in the intermolecular PES. But we do not know how effective this "motional averaging" is. So, to formulate the problem in a realistic way, we imagine that the attached CH_4 is a "structured" argon atom. In the limit of rapid, isotropic motion, the atom is a completely spherical object with a spherically distributed polarizability. As the motion slows down, the atom develops "structure," corresponding to the development of tetrahedrally oriented bonds to the four hydrogen atoms, and a similarly distributed polarizability. Thus, we write $\hat{V}(\theta,\phi,\chi)$ as a sum of two terms

$$\hat{V}(\theta,\phi,\chi)=(1-\rho)\hat{V}_{\mathrm{C}}+\rho\hat{V}_{\mathrm{H}}, \tag{7}$$

where

$$\hat{V}_{\mathrm{C}}=\sum_i 4\epsilon_i\left[\left(\frac{\sigma_i}{r'_{\mathrm{C}}-R_i}\right)^{12}-\left(\frac{\sigma_i}{r'_{\mathrm{C}}-R_i}\right)^{6}\right] \tag{8}$$

$$\hat{V}_{\mathrm{H}}=\sum_{\mathrm{H},i} 4\epsilon_i\left[\left(\frac{\sigma_i}{r'_{\mathrm{H}}-R_i}\right)^{12}-\left(\frac{\sigma_i}{r'_{\mathrm{H}}-R_i}\right)^{6}\right]. \tag{9}$$

Here, $\hat{V}_{\mathrm{C}}$ represents the contribution of the single carbon atom of the attached CH_4 to the total interaction energy. Similarly, $\hat{V}_{\mathrm{H}}$ represents the contribution of the four hydrogen atoms of the attached CH_4 to the total interaction energy.

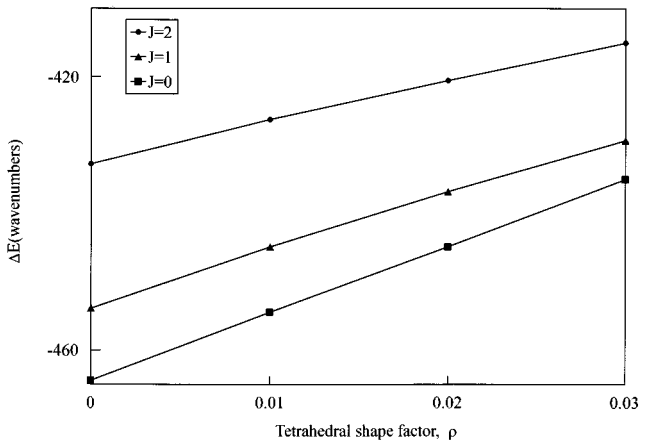

FIG. 5. The dependence of the lowest CH_4 internal rotor levels of each symmetry type on ρ, the tetrahedral shape factor (see text). $\rho=0$ corresponds to a freely rotating CH_4. Increasing values of ρ represent an increasing anisotropy of the interaction between the rotating CH_4 and the parent 1FN molecule.

Both types of interactions were modeled using the Ar–F, C, and H Lennard-Jones interaction parameters ϵ_i and σ_i.[27] The index i represents the 18 atoms of 1FN or 2FN. The vectors r'_C and r'_H are the 1/2FN principal axis vectors of the CH_4 atoms. These are related to the CH_4 principle axis vectors $r_{C,H}$ by the transformation

$$r'_{C,H}=\hat{U}r_{C,H}+t, \tag{10}$$

where $\hat{U}$ (θ,ϕ,χ) is the transformation matrix that relates the two principle axis systems and t is the translation vector that connects their centers-of-mass. *Ab initio* structures were assumed for CH_4, 1FN, and 2FN. The parameter ρ in Eq. (7), which we call a ''tetrahedral shape factor,'' is a weighting factor that partitions the CH_4–1/2FN dispersion interactions among the five CH_4 atoms. When $\rho=0$, the CH_4 is a structureless particle, with all of the dispersion attributed to a single center, the C atom, having an Ar-like polarizability. When $\rho\neq 0$, only the fraction $(1-\rho)$ is attributed to this center, and the fraction $(\rho/4)$ is attributed to each of the four attached H atoms. Clearly, $0<\rho<1$. The limit $\rho=0$ corresponds to an isotropically rotating CH_4. In this limit, we find a well depth of 465 cm^{-1} at $R=3.5$ Å, a reasonable result. Higher values of ρ correspond to a more structured CH_4, increasingly locked in some particular, energetically favorable position. But, of course, the real situation lies somewhere between these two limits.

We next evaluate the influence of ρ on the energies of the complex. Figure 5 shows the calculated energies of the lowest $J=0$, 1, and 2 rotational levels of CH_4 in CH_4–1FN as a function of ρ, the tetrahedral shape factor. (Qualitatively similar results were obtained for CH_4–2FN.) With $\rho=0$, corresponding to a freely rotating CH_4, the methane rotor levels exhibit their usual $2BJ(J+1)$ spacing, with the $J=0$ level lying at lowest energy ($V=-465$ cm^{-1}). But, as ρ increases from zero, the $J=0$, 1, and 2 levels are destabilized in energy. The extent of destabilization depends on J. The ''nonrotating'' $J=0$ methane is destabilized most; the more rapidly rotating $J=2$ methane is destabilized least. Thus, the separations of the $J=0$, 1, and 2 levels decrease with increasing ρ. The $J=0-1$ $(A-F)$ spacing decreases more rapidly than the $J=1-2(F-E)$ spacing; the $J=0$ and 1 levels become degenerate near $\rho\sim 0.05$. Since increasing values of ρ represent an increasing anisotropy of the interaction between the rotating CH_4 and the fixed 1FN, this means that higher values of J average out these anisotropies more effectively, for a given value of ρ. Clearly, at low values of ρ, the binding energy decreases with increasing J.

In our experiments, we measure the *difference* in the binding energy of a CH_4 to the S_0 and S_1 states of 1/2FN. The $S_1\leftarrow S_0$ transition conserves nuclear spin; hence, the three bands we observe are $A\leftrightarrow A(J=0)$, $F\leftrightarrow F(J=1)$, and $E\leftrightarrow E(J=2)$. These three bands should have relative intensities 5, 9, and 10, respectively. Different surfaces (i.e., different electronic states) may have different values of ρ. Since we know that the CH_4 is more strongly bound in the S_1 state, we expect that $\rho(S_1)>\rho(S_0)$. Thus, the separations of the $J=0$, 1, and 2 levels of the attached CH_4 should be smaller in the S_1 state than in the S_0 state of 1/2FN. This then leads to the prediction that the three bands will be energy ordered as $E\leftrightarrow E<F\leftrightarrow F<A\leftrightarrow A$, with relative intensities 10:9:5. Further, we expect that the spacing between the E and F subbands will be less than the spacing between the F and A subbands. Comparing these predictions to experiment, we find that this is exactly what is observed. In CH_4–1FN, the three bands (in order of increasing energy) have intensities 2:2:1 (±10%), with splittings of 0.23 and 0.93 cm^{-1}. In CH_4–2FN, the three bands also have intensities 2:2:1 (±10%), with splittings of 0.14 and 0.52 cm^{-1}. Notably, the ratio of the spacings is about the same in both complexes. In view of this agreement, we conclude that the appearance of three closely spaced 0_0^0 bands in the $S_1\leftarrow S_0$ excitation spectra of CH_4–1/2FN is indeed a consequence of a perturbation of the normally isotropic rotation of the methane molecule by the nearby surface. This leads to a van der Waals interaction energy that depends both on the rotational state of the CH_4 and on the electronic structure of the surface to which it is attached.

Numerical estimates of ρ can be obtained by simultaneously varying ϵ_i. Different values of ϵ_i may be required to reproduce the observed red shifts in the low resolution spectra, whereas different values of both ϵ_i and ρ may be required to reproduce the observed splittings in the high resolution spectra. The results of some typical calculations are shown in Fig. 6. We can reproduce the red shift in CH_4–1FN (-10.5 cm^{-1}) with $\epsilon_i(S_1)/\epsilon_i(S_0)=1.023$. We can reproduce the red shift in CH_4–2FN (-18.8 cm^{-1}) with $\epsilon_i(S_1)/\epsilon_i(S_0)=1.042$. And, based on the trends shown in Fig. 6, we can reproduce both the energy orderings and the spacings of the three components in both CH_4–1/2FN with ρ values of order 0.05. (Larger basis sets will be required to obtain more accurate values of ρ.) Clearly, since the values of ρ are nearly the same in both cases, the splittings in the spectra are primarily controlled by the differences in ϵ_i. In other words, the rotational motion of CH_4 is primarily controlled by the nature of the surface to which it is attached.

Some perspectives of the nature of this surface are provided by our calculations. Shown in Figs. 7–9 are one-dimensional slices of the intermolecular PES of S_0

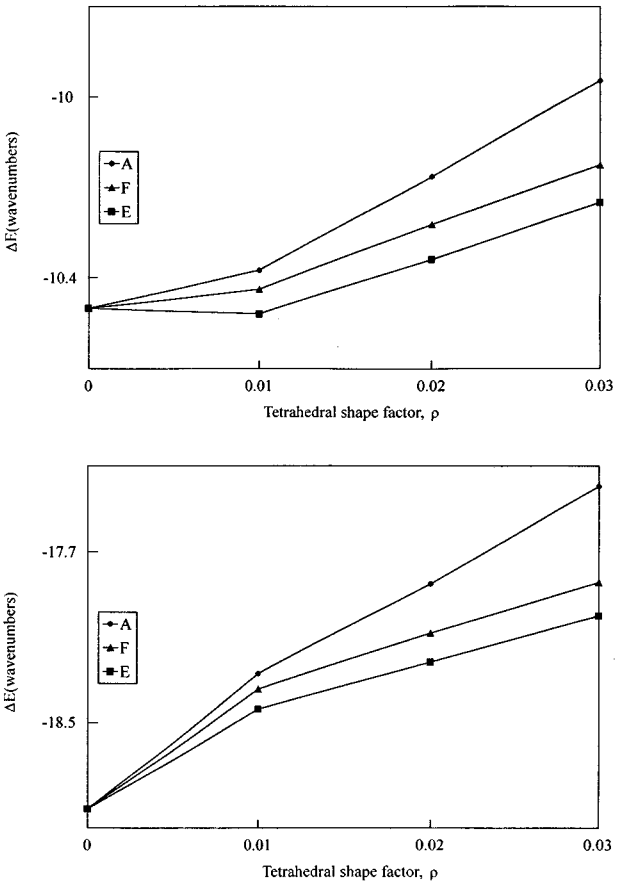

FIG. 6. Calculated ΔE values of the E,F, and A subbands of the CH_4–1FN (top) and CH_4–1FN (bottom) van der Waals complexes. In these calculations ρ was held constant for both the ground and excited states. An epsilon weighting factor of 1.023 (1FN) and 1.042 (2FN) was applied to the excited state to bring the calculated ΔE values into closer agreement with experiment.

CH_4–1FN along three angular coordinates. (ρ=0.015 was assumed in these calculations.) The most stable configuration of the methane molecule on top of either 1FN or 2FN is with three CH bonds ''down'' and one CH bond ''up,'' perpendicular to the aromatic plane ($\theta=\phi=0°$, $\chi=30°$). The perpendicular CH bond is a C_3 axis of the (undistorted) CH_4. Varying χ corresponds to a rotation of CH_4 about this axis. The one-dimensional surface along this coordinate (Fig. 7) is very ''soft,'' with a threefold barrier on the order of 1 cm^{-1}. In contrast, rotation of the CH_4 from a configuration in which three CH bonds are down to a configuration in which three CH bonds are up is relatively ''hard'' (Fig. 8). Finally, rotating the CH_4 in the latter configuration about its perpendicular C_3 axis requires very little energy, significantly less than 1 cm^{-1} (Fig. 9). At low values of ρ, the barriers scale approximately linearly with ρ. Thus, we conclude that, like the water molecule in H_2O–benzene,[28–31] the methane molecule in CH_4–1/2FN exhibits virtually free rotation about all of its axes. Only the ''top to bottom'' rotation is slightly hindered, a direct consequence of the steeper variation in V with z.

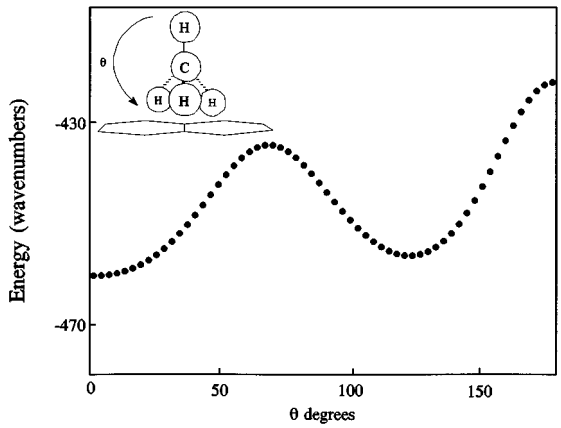

FIG. 8. The intermolecular potential for a model CH_4 internal rotor as a function of $\theta(\rho=0.015)$. The other two angular variables, χ and ϕ, are held fixed at 0°.

It is interesting to compare these results to those pertaining to ''real'' surfaces. Early IR studies showed that CH_4 adsorbed on a porous glass surface is most likely to rotate about a threefold axis, perpendicular to the plane.[32] Exchange of the H atoms in C–CH_3 among three equivalent sites on Pt(111) is fast on the NMR time scale but slow on the IR time scale.[33] Chemisorbed O–CH_3 on alumina apparently exhibits free rotation about the C–O bond axis.[34] Meth-

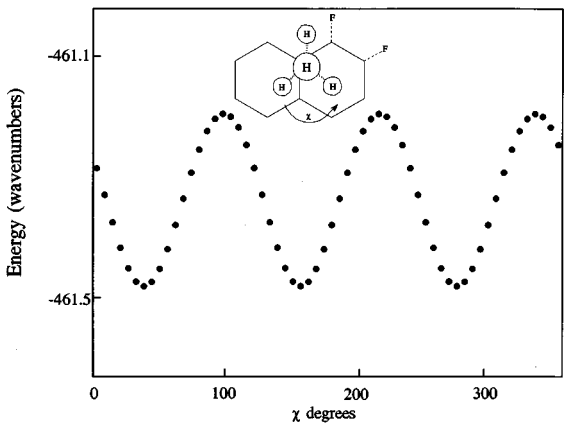

FIG. 7. The intermolecular potential for a model CH_4 internal rotor as a function of $\chi(\rho=0.015)$. The other two angular variables, θ and ϕ, are held fixed at 0°. The rotation takes place at the potential minimum in θ (see Fig. 8).

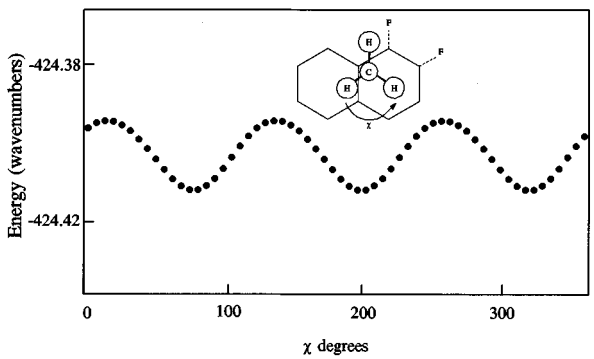

FIG. 9. The intermolecular potential for a model CH_4 internal rotor as a function of $\chi(\rho=0.015)$. The other two angular variables, θ and ϕ, are held fixed at 180° and 0°, respectively. The rotation takes place at the potential maximum in θ (see Fig. 8).

ane on MgO is bound ''dipod-down;'' the barrier to rotation about a threefold axis is 85 cm^{-1}.[35] And the equivalent rotation of methane on graphite requires overcoming a barrier of 200 cm^{-1}.[36] Thus, the methane molecules in CH_4–1/2FN are rotationally much more mobile than on ''real'' surfaces, more like an intrinsic mobile precursor state than a physisorbed (or chemisorbed) species. Even small molecule van der Waals complexes like H_2/D_2–HF,[37] CH_4–HCl,[21] and CH_4–H_2O[22] exhibit significantly larger barriers to internal rotation than $COCH_4$–1/2FN.

There is a direct connection between our treatment of CH_4–1/2FN and the treatment of hindered internal rotation in other systems.[38] We have in mind problems like the restricted rotation of a methyl group *covalently* bonded to an aromatic plane. Nuclear symmetries play an important role in both types of systems. Thus, the 0_0^0 band of the $S_1 \leftarrow S_0$ electronic spectrum of 1-methylnaphthalene (1MN) is split by the tunneling motion of the methyl group.[39] Two closely spaced vibronic bands are observed, $A \leftrightarrow A$ and $E \leftrightarrow E$, completely analogous to the $A \leftrightarrow A$, $E \leftrightarrow E$, and $F \leftrightarrow F$ bands of CH_4–1/2FN. Further, our ρ is completely analogous to the leading term in the usual Fourier expansion of hindered rotor potentials. Increasing the value of ρ clearly corresponds to increasing the value of the barrier to internal rotation. However, since ρ is small in CH_4–1/2FN, there is no preferred axis of internal rotation of the attached CH_4. No torsion-rotation perturbations appear in their electronic spectra. (1MN exhibits such perturbations in its $S_1 \leftarrow S_0$ spectrum.[39]) Further, no M (or K) splittings are observed in the spectra of CH_4–1/2FN, unlike the case of CH_4–HCl.[21] This is because the anisotropy of the intermolecular PES in the CH_4–1/2FN complexes is extremely small. (Such splittings appear in our calculations at higher ρ.) In this respect, then, a methane molecule in the vicinity of an aromatic ''surface'' is truly a ''floppy'' molecule.

ACKNOWLEDGMENTS

We thank S. A. DeForest for experimental assistance and G. T. Fraser, R. E. Miller, D. J. Nesbitt, M. Trenary, and J. T. Yates, Jr. for helpful discussions. This work has been supported by NSF (CHE-9224398).

[1] R. E. Smalley, L. Wharton, D. H. Levy, and D. W. Chandler, J. Chem. Phys. **68**, 2487 (1978).
[2] For reviews, see J. M. Hutson, Annu. Rev. Phys. Chem. **41**, 123 (1990); R. C. Cohen and R. J. Saykally, *ibid.* **42**, 369 (1991).
[3] J. O. Hirschfelder, C. F. Curtiss, and R. B. Bird, *Molecular Theory of Gases and Liquids* (Wiley, New York, 1965).
[4] W. A. Majewski, J. F. Pfanstiel, D. F. Plusquellic, and D. W. Pratt, in *Laser Techniques in Chemistry*, edited by T. Rizzo and A. D. Myers (Wiley, New York, 1995).
[5] W. A. Majewski, D. F. Plusquellic, and D. W. Pratt, J. Chem. Phys. **90**, 1362 (1989).
[6] J. R. Johnson, K. D. Jordan, D. F. Plusquellic, and D. W. Pratt, J. Chem. Phys. **93**, 2258 (1990).
[7] B. B. Champagne, Ph.D. thesis, University of Pittsburgh, 1994.
[8] J. K. G. Watson, in *Vibrational Spectra and Structure*, edited by J. R. Durig (Elsevier, Amsterdam, 1977), Vol. 6, p. 1, and references therein.
[9] W. Gordy and R. L. Cook, *Microwave Molecular Spectra*, 3rd ed. (Wiley–Interscience, New York, 1984).
[10] See, for example, Th. Weber and H. J. Neusser, J. Chem. Phys. **94**, 7689 (1991), and references therein.
[11] J. Kraitchman, Am. J. Phys. **21**, 17 (1953).
[12] B. B. Champagne, D. F. Plusquellic, J. F. Pfanstiel, W. M. van Herpen, and W. L. Meerts, Chem. Phys. **156**, 251 (1991).
[13] M. Mandziuk and Z. Bačić, J. Chem. Phys. **98**, 7165 (1993), and references therein.
[14] M. J. Frisch, M. Head-Gordon, G. W. Trucks, J. B. Foresman, H. B. Schlegel, K. Raghavachari, M. A. Robb, J. S. Binkley, C. Gonzalez, D. J. Defrees, D. J. Fox, R. A. Whiteside, R. Seeger, C. F. Melius, J. Baker, R. L. Martin, L. R. Kahn, J. J. P. Stewart, S. Topiol, and J. A. Pople, GAUSSIAN 90, Gaussian, Inc., Pittsburgh, Pennsylvania, 1990.
[15] T. Troxler and S. Leutwyler, J. Chem. Phys. **95**, 4010 (1991).
[16] D. O. DeHaan and T. S. Zwier, J. Chem. Phys. **90**, 1460 (1989).
[17] K. Yamanouchi, S. Isogai, and S. Tsuchiya, J. Mol. Struct. **146**, 349 (1986); B. Coutant and P. Brechignac, J. Chem. Phys. **91**, 1978 (1989).
[18] S. A. Wittmeyer, T. Troxler, and M. R. Topp, J. Phys. Chem. **97**, 10 613 (1993).
[19] G. Herzberg, *Electronic Spectra of Polyatomic Molecules* (van Nostrand, Princeton, 1966).
[20] E. B. Wilson, Jr., J. Chem. Phys. **3**, 276 (1935).
[21] Y. Oshima and Y. Endo, J. Chem. Phys. **93**, 6256 (1990).
[22] L. Dore *et al.*, J. Chem. Phys. **100**, 863 (1994); R. D. Suenram, G. T. Fraser, F. J. Lovas, and Y. Kawashima, J. Chem. Phys. **101**, 7230 (1994).
[23] R. W. Randall, J. B. Ibbotson, and B. J. Howard, J. Chem. Phys. **100**, 7051 (1994).
[24] See, for example, V. Buch and J. P. Devlin, J. Chem. Phys. **98**, 4195 (1993), and references therein.
[25] R. N. Zare, *Angular Momentum* (Wiley–Interscience, New York, 1988).
[26] W. H. Press, B. P. Flannery, S. A. Teukolsky, and W. T. Vetterling, *Numerical Recipes in C* (Cambridge University, Cambridge, 1988).
[27] D. Consalvo, A. van der Avoird, S. Piccirillo, M. Coreno, A. Giardini-Guidoni, A. Mele, and M. Snels, J. Chem. Phys. **99**, 8398 (1993).
[28] A. J. Gotch and T. S. Zwier, J. Chem. Phys. **96**, 3388 (1992).
[29] J. D. Augspurger, C. E. Dykstra, and T. S. Zwier, J. Phys. Chem. **96**, 7252 (1992).
[30] S. Suzuki, P. G. Green, R. E. Baumgarner, S. Dasgupta, W. A. Goddard, III, and G. A. Blake, Science **257**, 942 (1992).
[31] H. S. Gutowsky, T. Emilsson, and E. Arunan, J. Chem. Phys. **99**, 4883 (1993).
[32] N. Sheppard and D. J. C. Yates, Proc. R. Soc. Ser. A **238**, 69 (1956).
[33] I. J. Malik, M. E. Brubaker, S. B. Mohsin, and M. Trenary, J. Chem. Phys. **87**, 5554 (1987).
[34] T. P. Beebe, Jr., J. E. Crowell, and J. T. Yates, Jr., J. Chem. Phys. **92**, 5119 (1990).
[35] J. Z. Larese, J. M. Hastings, L. Passell, D. Smith, and D. Richter, J. Chem. Phys. **95**, 6997 (1991).
[36] M. V. Smalley *et al.*, Mol. Phys. **44**, 533 (1981).
[37] C. M. Lovejoy, D. D. Nelson, and D. J. Nesbitt, J. Chem. Phys. **87**, 5621 (1987); **89**, 7180 (1988).
[38] L. H. Spangler and D. W. Pratt, in *Jet Spectroscopy and Molecular Dynamics*, edited by J. M. Hollas and D. Phillips (Chapman and Hall, London, 1995).
[39] X.-Q. Tan, W. A. Majewski, D. F. Plusquellic, and D. W. Pratt, J. Chem. Phys. **94**, 7721 (1991).